

# Enhanced efficiency of dye sensitized solar cell by doping Ba into TiO<sub>2</sub> nanoparticle

Amutha M<sup>1</sup>, Ramkumar G<sup>2</sup>

<sup>1</sup>Assistant Professor, Department of Physics, Devanga Arts College, Aruppukottai, Virudhunagar 626101, Tamilnadu, India

<sup>2</sup>Research Scholar, Department of Renewable Energy Science, Manonmaniam Sundaranar University, Tirunelveli, 627012, Tamilnadu, India

**Abstract**—Pure TiO<sub>2</sub> and Barium (0.7 wt%) doped TiO<sub>2</sub> (BaTiO<sub>2</sub>) photoanodes have been synthesized by the facile microwave irradiated method. The pure anatase phase of synthesized photoanodes were confirmed by X-ray diffraction patterns. Ba doping in the TiO<sub>2</sub> host structure influenced the optical band gap which was studied by Uv-visible spectroscopy. The optical band gap was increased from 3.21 eV for the TiO<sub>2</sub> to 3.26 eV for BaTiO<sub>2</sub>. From the scanning electron microscopy, the particle shape morphology was observed for both TiO<sub>2</sub> and BaTiO<sub>2</sub> photoanodes. Barium presence in the TiO<sub>2</sub> host was endorsed by energy dispersive x-ray spectroscopy (EDS). No other impurities peaks were observed in the synthesized TiO<sub>2</sub> and BaTiO<sub>2</sub> photoanodes which also confirmed by EDS. Electrochemical impedance spectroscopy shows the charge transfer resistance value was increased for BaTiO<sub>2</sub> which helps to reduce the dark current creation in dye sensitized solar cell. BaTiO<sub>2</sub> photoanode have 3.24 % conversion efficiency and TiO<sub>2</sub> photoanode have 2.1% conversion efficiency.

**Index Terms**—DSSC, Photoanode, Low cost dye, Microwave irradiated method.

## I. INTRODUCTION

The world needs green and cost effective technology for energy sector owing to the global greenhouse effect and depletion of fossil fuels in recent years. Among all the existing green energy technologies such as wind turbines, hydropower, tidal power, solar thermal and biomass, the solar cell is considered as the most promising and prominent energy [1-3]. A dye-sensitized solar cell (DSSC) is a potential one to compare other generation solar cells because the cheap cost, comparable power conversion efficiency (PCE) and easy fabrication method [4-6]. The highest PCE 13% of DSSC has been achieved by using ruthenium dye [7]. The effective methods to enhance

the performance of DSSC are mainly based on minimizing photo-generated electron-hole recombination in the semiconducting metal oxide of DSSC and improving transfer rate of photo-generated electrons in the transparent conducting substrate [8, 9]. This photo-generated electron transfer rate mainly depends the band gap of the semiconducting metal oxide, which is compactable to the dye molecule, to increase the dye loading in semiconducting metal oxide surface and electrolyte diffusion in the photoanode respectively [10].

TiO<sub>2</sub> nanostructures are the most important photoanode materials because of its superior properties such as wide band gap, non-toxicity, low cost and highly stable [11-12]. The desired things for the efficiency of the DSSC solar cells is size, morphology, microstructure and surface crystal plane. From this point of view, we have to design with this quality during the TiO<sub>2</sub> material for the DSSC performance improvement [13].

The improvement of DSSC solar cells were made by using the TiO<sub>2</sub> nanostructures, combination of carbon spheres. TiO<sub>2</sub> micro tablets, hollow spheres, nanofibers nanoparticle composites and nanotube-nanoparticle composite were also used as a photoanode material for the performance enhancement of the DSSC solar cells [14-17]. Hence, doping of TiO<sub>2</sub> with transition metal, rare earth and noble metal ion have been investigated widely to reduce the particle size. It enhances the surface area of TiO<sub>2</sub> nanoparticles and also modifies the optical absorption properties of the TiO<sub>2</sub>. Vijayalakshmi et al have reported, the barium doping in TiO<sub>2</sub> nanoparticles using microwave irradiated method which increase the optical band gap and reduce the particle size of

the  $\text{TiO}_2$  nanoparticle for microbiological activity [18].

From this time, the present work deals with the synthesizing of  $\text{TiO}_2$  and  $\text{BaTiO}_2$  photoanode using facile microwave irradiated method. Structural, optical, morphological, elemental and electrochemical behavior of synthesized photoanodes are investigated. Photovoltaic performance of synthesized  $\text{TiO}_2$  and  $\text{BaTiO}_2$  photoanodes are investigated by photocurrent-voltage characteristic. Increasing the optical band gap and surface area of  $\text{BaTiO}_2$  photoanode exhibits reduction of dark current production and increases the dye loading capacity of DSSC along with it also increases the PCE of DSSC [19].

## II. EXPERIMENTAL DETAILS

Titanium (IV) isopropoxide TTIP (95% of purity), Ruthenium dye (N3 dye), Polyethylene glycol (PEG), Barium chloride and Triton X- 100 were purchased from Alfa Aesar Company from India. Ethanol was purchased from Merck Company from India. Chloroplatinic acid, 99.9% was purchased from Himedia Company from India. All the chemicals were used without purification. Deionized (DI) water was used in all the experiments. Facile microwave irradiated method was used to prepare  $\text{Ba}_x\text{TiO}_2$  ( $x=0$  & 0.7) photoanode materials. Solution preparation details are follows: first step is to prepared first solution, 2g of TTIP added with 60 ml of DI water. Second step is stirred prepared first solution for 1 hr at 100 °C. Step three is to prepare the second solution, barium chloride dissolved with DI water. In this third step solution is prepared in separate. Fourth step is to add first and second solution and stirred 1 hr and solution is subjected to the microwave oven treatment for 5 min at 450 W power. Microwave irradiation offers rapid and uniform heating of the reaction medium and thus provides uniform nucleation and growth conditions for photoanode materials. Fifth step is calcination at 500 °C for 2 hr. This calcination process is help to improve the crystalline nature material. This same process flow is follows for the preparation of  $\text{TiO}_2$ . Device fabrication process steps are follows: first step is FTO glass plates cleaning. Soap solution, distilled water and ethanol are used for FTO cleaning process. Second step is synthesized photoanode material is added with binder solutions PEG and Triton X-100.

At this end of the second step prepared material get in to the paste form, Third step is prepared paste the coated in to the FTO by using the doctor blade technique. Fourth step is sintering at 400 °C for 1 hr. when the sintering the binder solution get evaporation. Fifth step is ruthenium dye (0.5 mM) immersion. In this dye immersion is done for 24 hr. In this dye molecule are called as photo-electrode. Sixth step is counter electrode coating process. Platinum is coated by using the 5Mmol chloroplatinic acid. Seventh step is to connect (Sandwiched type) the photo electrode and counter electrode with the help of binder clips. Eight step is liquid electrolyte injection. potassium iodide (KI) and iodine ( $I_2$ ) is injected in between the photo-electrode and counter electrode. KI and  $I_2$  dissolved using the acetonitrile as electrolyte. The device area is 0.25  $\text{cm}^2$ .

### *Characterizations*

XRD studies were conducted on an X-ray powder diffraction instrument (PANalytical X'pert pro powder diffractometer using  $\text{CuK}\alpha$  radiation,  $\lambda=1.54$  Å) for synthesized photoanode with  $2\theta$  range values from 10° to 80°. The measurement was carried out by step size of 0.0170° with four decimal accuracy. SEM images of photoanode materials were taken by ZEIS EVO 18 instrument with 20 kV acceleration voltage and 1.30 K magnification. The ultraviolet-visible (UV-Vis) absorption spectra were recorded in a Perkin Elmer Lambda 35 spectrophotometer. EIS were conducted by VSP300 biological instrument with a 10 mV voltage amplitude in the frequency range of 1MHz-1Hz. The Photocurrent-Voltage(I-V) characteristics was carried out by means of a computer controlled electrochemical workstation and SAN-EI solar stimulator, 150 W Xenon lamp was used as light source with AM 1.5 G filter which has an intensity of 100 mW/cm<sup>2</sup>.

## III. RESULT AND DISCUSSIONS

The powder X-ray diffraction pattern of  $\text{TiO}_2$  and  $\text{BaTiO}_2$  photoanode materials are shown in the Fig. 1.  $\text{TiO}_2$  and  $\text{BaTiO}_2$  photoanodes are very well matched with JCPDS data (21-1272). No other characteristic peaks reflected in X-ray diffraction pattern. Hence, both samples exhibit tetragonal structure and corresponding lattice constant values are shown in Table 1. The ionic radius of  $\text{Ba}^{2+}$  is 1.42 nm and  $\text{Ti}^{4+}$  is 0.74 nm. From the XRD the intensity is reduced in Fig.1c compared the Fig.1b.

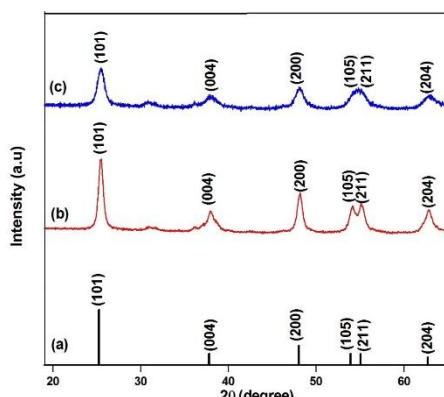


Fig.1 X-ray diffraction pattern of (a) JCPDS data 21-1272, (b) TiO<sub>2</sub> photoanode (c) BaTiO<sub>2</sub> photoanode. This is because of Ba<sup>2+</sup> substitute into the TiO<sub>2</sub> host photoanode lattice. The ionic radius of Ba<sup>2+</sup> is higher than Ti<sup>4+</sup>. In this help to control the particle size. During the substitution distortion and inflation may happen in the TiO<sub>2</sub> photoanode crystal lattice, it will reduce the nucleation growth [20].

The structural properties are calculated by the following equation [21]:

where d is the d-spacing between two consecutive lattice observed from X-ray diffraction, (h,k,l) are miller indices, a, b, and c are lattice constant for a=b in tetragonal structure, t, λ, β and θ are corresponding to the crystallite size, wavelength of the X-ray used, full with half maximum and diffraction angle.

$$\frac{1}{d^2} = \frac{h^2 + k^2}{a^2} + \frac{l^2}{c^2} \quad (1)$$

$$t = \frac{0.9\lambda}{\beta \cos\theta} \quad (2)$$

where d is the d-spacing between two consecutive lattice observed from X-ray diffraction, (h,k,l) are miller indices, a, b, and c are lattice constant for a=b in tetragonal structure, t, λ, β and θ are corresponding to the crystallite size, wavelength of the X-ray used, full with half maximum and diffraction angle. where, n is four for anatase phase TiO<sub>2</sub> and 2 for rutile phase TiO<sub>2</sub>. ρ, M, N, V, S<sub>a</sub> are corresponding to the density of the prepared sample, molecular weight of the prepared photoanodes, avagedra constant value, volume of the prepared photoanodes and states the specific surface of the prepared sample. In Table 1 the calculated structural properties are listed.

The average crystallite sizes of pure TiO<sub>2</sub> and BaTiO<sub>2</sub> corresponding to the 16 nm and 25 nm. This because of barium substitution with the TiO<sub>2</sub>. This substitution reduced the nucleation and reduce the growth rate of the TiO<sub>2</sub>. Therefore, the particle size of BaTiO<sub>2</sub> photoanode is reduced.

$$\rho = \frac{nM}{NV} \quad (3)$$

$$S_a = \frac{6}{D \cdot \rho} \quad (4)$$

If we reduced the particle size the surface area will increase. Specific surface area of TiO<sub>2</sub> photoanode ( $6.12 \times 10^5$  g cm<sup>-2</sup>) was greater than the BaTiO<sub>2</sub> ( $9.57 \times 10^5$  g cm<sup>-2</sup>) photoanode. If the specific area is high it will absorbed more die. It will help to generate more photo-current in the DSSC.

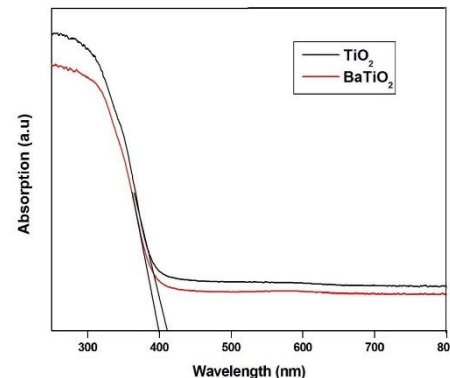


Fig. 2 UV-visible spectroscopy of synthesized TiO<sub>2</sub> and BaTiO<sub>2</sub> photoanodes

Absorption spectrum of the TiO<sub>2</sub> and BaTiO<sub>2</sub> is show in Fig. 2. BaTiO<sub>2</sub> have more absorption below the 400 nm. This indicate the absorption changes in TiO<sub>2</sub> due to the metal doping. BaTiO<sub>2</sub> have regular absorption and slight blue shift compared to TiO<sub>2</sub>. This blue shift in the absorption edge represent the Burstein Moss effect, it leads to the motion of fermi level towards conduction band. This due to the barium doping, when the barium doping electron concentration is increase [22, 23]. It is main factor for the improvement of photocurrent density and charge transfer resistance.

The absorption edges of TiO<sub>2</sub> is 415 nm and absorption edges of BaTiO<sub>2</sub> is 400 nm. The band gap values are determined by using tauc plot (see in Fig. 3). Band gap values are calculated using the relation (see in eq. 5.). BaTiO<sub>2</sub> photoanode (3.21 eV) has

highest band gap value compared to  $\text{TiO}_2$  photoanode (3.26 eV) because of quantum confinement effect.

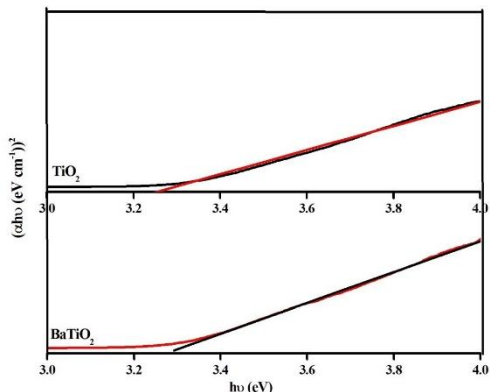


Fig. 3 Tauc plot of synthesized  $\text{TiO}_2$  and  $\text{BaTiO}_2$  photoanodes

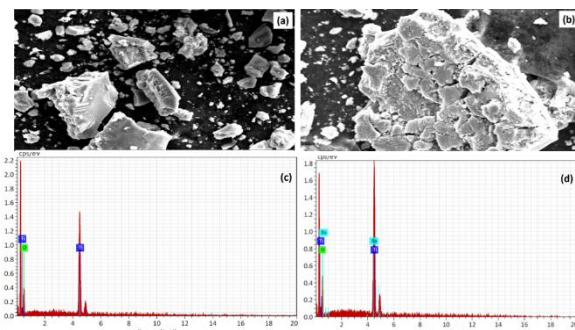


Fig. 4 SEM image of (a)  $\text{TiO}_2$  and (b)  $\text{BaTiO}_2$  photoanodes and EDX of (c)  $\text{TiO}_2$  and (d)  $\text{BaTiO}_2$

The morphological image of  $\text{TiO}_2$  and  $\text{BaTiO}_2$  are shown in Fig 4. Both,  $\text{TiO}_2$  and  $\text{BaTiO}_2$  have same agglomeration of spherical shape particle. The composition confirmation is done by the EDS. Ti and O are confirmed in the as prepared  $\text{TiO}_2$  material with free impurities. Barium is confirmed in the  $\text{BaTiO}_2$  photoanode. Ti and O confirmation is shows Fig 4a and Barium confirmation is shows in Fig 4b.

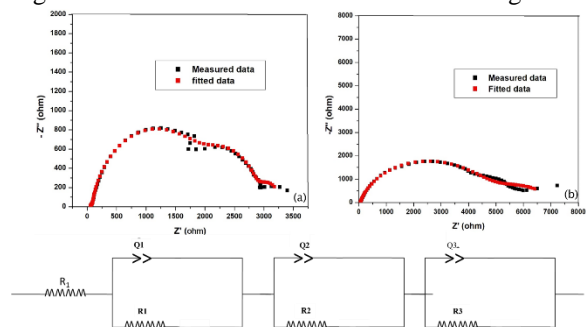


Fig. 5 EIS of synthesized (a)  $\text{TiO}_2$  and (b)  $\text{BaTiO}_2$  photoanode and (c) is the equivalent circuit of corresponding EIS.

The interfacial reaction kinetics in the DSSC was further confirmed using the EIS result. The EIS spectra of  $\text{TiO}_2$  and  $\text{BaTiO}_2$  photoanodes under the dark condition with 0.6 V open circuit voltage are depicted in Fig.5. DSSC electrochemical behavior is explain in the three frequency range such as: high, middle and low. In the high frequency range semicircle endorsed to the electrochemical reaction occurred in platinized counter electrode and the electrolyte interface (charge transfer resistance  $R_{ct}$  1). The appearance of semicircle in the middle frequency region is due to the electron transfer resistance within the  $\text{TiO}_2$  film and the possible reverse reaction at  $\text{TiO}_2$ /electrolyte interface (charge transfer resistance  $R_{ct}$  2). Associated charge transfer in electrolyte (Nernst diffusion) impacts the lower frequency region which is evident from the third semicircle. From the fitted data, The  $\text{BaTiO}_2$  photoanode charge transfer resistance value is higher than the  $\text{TiO}_2$  photoanode charge transfer resistance value. Barium doping increase the band gap value (which also confirmed by optical analysis) and this reduces the electron recombination in  $\text{BaTiO}_2$ /electrolyte interface. This behavior is attributed to the charge transfer value increment. The increment of charge transfer resistance is helpful to reduce the recombination result which evident for the photocurrent increment.

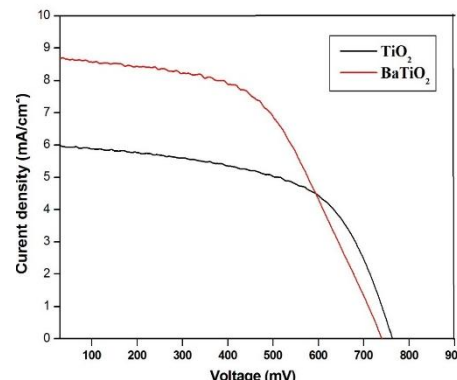


Fig. 6 Photovoltaic characterization of synthesized  $\text{TiO}_2$  and  $\text{BaTiO}_2$  photoanodes

The photovoltaic performance of fabricated DSSC is shown in the Fig. 6. Photocurrent density of  $\text{BaTiO}_2$  is higher than the  $\text{TiO}_2$  photoanode. This increment is due to the more photon absorption of dye molecule.  $\text{BaTiO}_2$  photoanode has the high surface area compared to the  $\text{TiO}_2$  photoanode which leads to the enhance dye loading capacity. This results are also

confirmed by the XRD and UV analysis. Another important phenomena of increment of photocurrent density is authorized by recombination rate or dark current reduction. BaTiO<sub>2</sub> photoanode has the high recombination resistance compare to the TiO<sub>2</sub> photoanode which reduce dark current production between the semiconducting metal oxides and electrolyte. Therefore, the BaTiO<sub>2</sub> photoanode (3.4 %) has highest PCE compared to TiO<sub>2</sub> photoanode (2.1 %). The calculated photovoltaic parameters are shown in Table 2.

**Table 1** the structural parameters derived from XRD pattern of synthesized TiO<sub>2</sub> and BaTiO<sub>2</sub> photoanode

Sl. No.	Sample	FWHM ( $2\theta$ )	d- spacing ( $\text{\AA}$ )	Crystallite size(D) (nm)	Lattice constant ( $\text{\AA}$ )		Unit cell Volume $V (\text{\AA})^3$	Density ( $\rho$ ) ( $\text{g}/\text{cm}^3$ )	Specific Surface area ( $\times 10^5$ $\text{g}/\text{cm}^2$ )
					a=b	c			
1.	TiO <sub>2</sub>	0.56828	3.494	25	3.778	9.480	135.31	3.919	6.12
2.	BaTiO <sub>2</sub>	0.87609	3.504	16	3.781	9.470	135.38	3.919	9.57

**Table 2** Photovoltaic parameters derived from J-V characterization of synthesized TiO<sub>2</sub> and BaTiO<sub>2</sub> photoanode

Sl. No.	Sample	J <sub>sc</sub> (mA/cm <sup>2</sup> )	V <sub>oc</sub> (mV)	FF	Efficiency (η) (%)	Ref
1.	TiO <sub>2</sub>	5.96	761	48	2.1	Present work
2.	BaTiO <sub>2</sub>	8.70	740	53	3.4	Present work
3.	TiO <sub>2</sub>	2.53	650	63	1.03	Ref 24
4.	W doped TiO <sub>2</sub>	4.77	730	71	2.47	Ref 24

#### IV. CONCLUSION

Barium is successfully incorporated with the TiO<sub>2</sub> with 0.7 weight percentage by using the microwave irradiated method. Prepared TiO<sub>2</sub> and BaTiO<sub>2</sub> photoanode have been coated on FTO by using the Doctor Blade technique. Than dye and counter electrode is added. Grain size is calculated by the Peak fit software with the XRD data. From the XRD, Ba decrease the grain size it leads to increase the specific surface. Higher surface area have higher die absorption, it will help to generate more photocurrent in DSSC. From the UV-Vis spectroscopy bandgap have been estimated. Bandgap of TiO<sub>2</sub> photoanode is 3.17 eV and Bandgap of BaTiO<sub>2</sub> photoanode is 3.23 eV. In the absorption spectrum edge shift is occurring towards lower wavelength. This shift indicate increase of bandgap due to the Ba incorporation. Elemental presence such as Ti, O and Ba are confirmed by the EDAX studies. These are

confirmed without any impurities and this confirmation done with XRD. The efficiency of BaTiO<sub>2</sub> photoanode DSSC is 3.4 %. It is 63% higher than the TiO<sub>2</sub> DSSC. Main factor for this improvement is due to the Ba incorporation with the TiO<sub>2</sub>. This incorporation reduces the particle and increase the surface area.

#### REFERENCES

- [1] F. Perera “Pollution from Fossil-Fuel Combustion is the Leading Environmental Threat to Global Pediatric Health and Equity: Solutions Exist”, Int. J. Environ. Res. Public Health, 15 (2018) 16.
- [2] L. S. Tiewsoh, J. Jirásek, M. Sivek “Electricity Generation in India: Present State, Future Outlook and Policy Implications”, Energies, 12 (2019) 1361.
- [3] Government of India “Monthly Policy Review – June 2018”. <https://www.prssindia.org/policy-review/monthly-policy-review>.
- [4] M. Z. Jacobson, M. A. Delucchi “Providing all global energy with wind, water, and solar power, Part I: Technologies, energy resources, quantities and areas of infrastructure, and materials”, Energy Policy, 39 (2011) 1154.
- [5] W. A. Badawy “A review on solar cells from Si-single crystals to porous materials and quantum dots”, J. Adv. Res., 6 (2015) 123.
- [6] S. Irvine “Solar Cells and Photovoltaics”, Springer Handbook of Electronic and Photonic Materials, 1 (2017) 1.
- [7] M. Gul, Y. Kotak, T. Munir “Review on recent trend of solar photovoltaic technology”, Energy Exploration & Exploitation 34 (2016) 485.
- [8] A. Morales-Acevedo, G. Casados-Cruz “Forecasting the Development of Different Solar Cell Technologies”, Int. J. Photoenergy., 1 (2013) 1.
- [9] K. Sharma, V. Sharma, S. S. Sharma “Dye-Sensitized Solar Cells: Fundamentals and Current Status” Nanoscale Res. Lett., 13 (2018) 381.
- [10] S. Bose, V. Soni, K. R. Genwa “Recent Advances and Future Prospects for Dye Sensitized Solar Cells: A Review” IJSER, 5 (2015) 2250.

- [11]. Q. Yu, Y. Pang and Q. Jiang “NiS submicron cubes with efficient electrocatalytic activity as the counter electrode of dye-sensitized solar cells” R. Soc. Open Sci., 5 (2018) 180186.
- [12] A. Carella, F. Borbone, R. Centore “Research Progress on Photosensitizers for DSSC” Frontiers in Chemistry, 6 (2018) 481.
- [13] A. Mishra, M. K. R. Fischer, P. Buerle “Metal-Free Organic Dyes for Dye-Sensitized Solar Cells: From Structure: Property Relationships to Design Rules”, Angew. Chem. Int. Ed., 48 (2009) 2474.
- [14] M. S. Suait, M. Y. A. Rahman, A. Ahmadc “Review on polymer electrolyte in dye-sensitized solar cells (DSSCs)”, Solar Energy, 115 (2015) 452.
- [15] H. Wang, Y. H. Hu, “Graphene as a counter electrode material for dye-sensitized solar cells” Energy & Environmental Science, 8 (2012) 1.
- [16] F. Labat, I. Ciofini, H. P. Hratchian, M. J. Frisch, K. Raghavachari, C. Adamo “Insights into Working Principles of Ruthenium Polypyridyl Dye-Sensitized Solar Cells from First Principles Modeling” J. Phys. Chem. C, 115 (2011) 4297.
- [17] D. Li, D. Zheng, J. Shi “DSSC-Integrated Glassblocks for the Construction of Sustainable Building Envelopes”, Adv. Mater. Res., 875 (2014) 629.
- [18] R. S. Devi, R. Venkatesh, R. Sivaraj,” Synthesis of Titanium Dioxide Nanoparticles by Sol-Gel Technique”, IJIRSET 3 (2014) 15206.
- [19] K. Vijayalakshmi, D. Sivaraj, “Synergistic antibacterial activity of barium doped TiO<sub>2</sub> nanoclusters synthesized by microwave processing”, RSC Adv., 6 (2016) 9663.
- [20] S. K. S. Patel, N. S. Gajbhiye, S. K. Date, “Ferromagnetism of Mn-doped TiO<sub>2</sub> nanorods synthesized by hydrothermal method”, J Alloys Compd., 509 (2011) 427.
- [21] K. N. Konou, Y. Lare, M. Haris, M. Baneto, K. A. Amou, K. Napo, “Influence of barium doping on physical properties of zinc oxide thin films synthesized by SILAR deposition technique”, Adv. Mater., 6 (2014) 63.
- [22] G. Cheng, F. Xu, F. J. Stadler, R. Chen, “A facile and general synthesis strategy to doped TiO<sub>2</sub> nanoaggregates with a mesoporous structure and comparable property”, RSC Adv., 5, (2015) 64293.
- [23] T. S. Moss, “The Interpretation of the Properties of Indium Antimonide”, Proc. Phys. Soc., London, Sect. B, 67 (1954) 775.
- [24] K. A. Bhabu, A. K. Devi, L. Theerthagiri, J. Madhavan, T. Balu, T. R. Rajasekaran, “Tungsten doped titanium dioxide as a photoanode for dye sensitized solar cells ”, J Mater Sci: Mater Electron, 28 (2016) 3428. communications channel equalization using radial basis function networks,|| IEEE Trans. on Neural Networks, vol. 4, pp.570-578, July 1993.